RSC Advances

1   **A DFT/ TDDFT Mission to Probe Push-Pull Vinyl Coupled**

2   **Thiophene Oligomers for Optoelectronic Applications**

3   Duraikannu Gajalakshmi[1], Rajadurai Vijay Solomon[2†], Venkatachalam Tamilmani[3*],

4   Mariasusai Boobalan[4], Ponnambalam Venuvanalingam[2*]

5

6   [1] Department of Chemistry, University College of Engineering Villupuram (A Constituent

7   College of Anna University, Chennai), TN, India.

8   [2]Theoretical and Computational Chemistry Laboratory, School of Chemistry, Bharathidasan

9   University, Tiruchirappalli- 620024, India.

10   [†]*Present address:* Department of Chemical Engineering, University of South Carolina,
11   Columbia, USA.
12
13   [3]Department of Chemistry, University College of Engineering Ariyalur (A Constituent

14   College of Anna University, Chennai), TN, India.

15   [4]Department of Chemistry, St.Joseph's College, Tiruchirapalli, TN, India.

16

17

18

19

20

21

22

23

Abstract

Vinyl coupled thiophene oligomer (VCTO) is one of the active components in organic solar cells. In the present study, VCTOs with various acceptor groups (-CN, -NO$_2$ & -COOH) have been considered and their optoelectronic properties evaluated using DFT/TDDFT calculations. Totally 17 VCTOs including 3 already reported, have been considered. The computed results reveal that the reference VCTOs (VCTO1, 2 & 3) can be used as possible electron transport materials and newly designed VCTOs are found to be promising hole transport materials. Among these, VCTO4b is found to show lower band gap whereas VCTO3c has higher band gap. Further the study explores the role of donor and acceptor groups on the band gap, ionization potential, electron affinity, exciton binding energy and light harvesting efficiency of these VCTOs. The spectral analysis shows that modelled VCTOs have a strong n→π*transition while the reference VCTOs found to show predominant π→π* transition. In summary, 9 out of 14 designed VCTOs are found to show better optoelectronic properties than their reference molecules.

46   **1.0 Introduction:**

47   The design and development of renewable energy sources using organic

48   solar cells (OSC) in recent years attract considerable interest due to increasing

49   energy demand[1-7]. Owing to large surface area and porous structure, metal

50   organic framework (MOF) and covalent organic framework (COF) has been the

51   subject of research in gas storage and catalysis[8-12]. Quantum chemical

52   calculations have been used to understand not only the nature of MOFs/COFs

53   (both in ground and excited states) but also the character of bands.[13-20] A unique

54   blend of optical and electronic properties of them has led to associating them in

55   the areas of photo catalytic, photovoltaic and electrochemical devices[21, 22]. The

56   OSC research is currently undergoing rapid growth due to its cost effective

57   production by vacuum processing on flexible substrates and higher power

58   conversion efficiency (PCE) of 10.7% in an active area of $1.1 cm^{2, 23}$. Typically,

59   in solution processed solar cells, with nano phase separated blend of a

60   semiconducting polymer as the donor and soluble fullerene as the acceptor

61   affords PCE exceeding 8%[24]. In this context, OSC made from π- conjugated

62   oligomer or dye appears as one of the promising materials in the conversion of

63   solar energy into electricity. The intensive research effort to prepare conjugated

64   poly heterocycles by electro polymerisation was originated in 1979[25]. Poly

65   pyrrole was prepared using pyrrole by electro polymerisation method[25, 26]. Later

66   on this was extended to thiophene[27-29], furan[30], indole[31], carbazole[32], benzene[33]

67   and fluorene[34]. Among these poly heterocycles, thiophene oligomer is one of the

68   subjects of considerable interest due to its simple structure and they were used

69   as models[35-40], to study electronic properties of poly thiophene[41-47]. So, the uses

70   of thiophene based molecules are inevitable in the material fabrication for solar

71   cells[48]. Recent developments in small molecule organic solar cells (SMOSC)

72   mainly use these conjugated oligomers[49].

73   Recently a series of π- conjugated oligomers were synthesized by Peter

74   Bauerle *et al.*[23] and reported to have high PCE of 6.9%. They have synthesized

75   a novel series of π-conjugated vinyl coupled thiophene oligomer (VCTO),

76   which is an electron withdrawing molecule, containing –CN group on either

77   side of the molecule for photovoltaic (PV) applications[23]. It is well known that

78   thiophene oligomers have excellent conjugation, planarity and rigidity in the

79   ring but are flexible for tuning their structure for better Photo Voltaic

80   performance. This prompted us to substitute various electron releasing and

81   withdrawing groups and screen various VCTOs for their optoelectronic

82   properties. Particularly, the role of electro releasing group, electron withdrawing

83   group and π-bridge on their optoelectronic properties was analyzed using

84   modern computational tools. A set of molecules have been designed with

85   electron releasing group and electron withdrawing group at the terminal end of

86   VCTOs and their suitability for better optoelectronic applications are examined.

87   Their properties have been computed and compared with available experimental

88   results.

89   In this work, the structure and properties of VCTOs have been

90   systematically analyzed via quantum chemical calculations using density

91   functional theory (DFT) and time dependent density functional theory (TDDFT)

92   methods. The optimized geometries, electronic properties, frontier molecular

93   orbital analysis (FMO), energy gap, ionization energy (IP), electro affinity

94   (EA), light harvesting efficiency (LHE), excitation binding energy (E_b),

95   hyperpolarizabillity(β^o) and charges have been calculated and analyzed. The

96   NBO analysis helps to ascertain the most stable donor-acceptor interaction in

97   these molecules and the effect of solvation has been studied using Polarizable

98   Continuum Model (PCM) calculations. The results are discussed one by one

99   here.

2.0 Computational Details

101   The structures of various thiophene oligomers chosen for the work are

102   shown in **figure 1**. B3LYP[50, 51] is known to perform well for most of the

103   organic molecules and therefore the same is adopted here[52-54]. The ground state

104   geometries of the molecule have been optimized using hybrid exchange-

105   correlation B3LYP functional with the 6-31g (d) basis set. All stationary points

106   have been confirmed as minima in the potential energy surface (PES) by

107   frequency analysis. The computed and experimental values for bond length and

108   angles are in agreement which emphasize the reliability of DFT method [SIT1].

109   First order hyper polarizability has been computed to check the NLO response

110   of the molecules. The first order hyper polarizability (β_0) has been calculated at

111   the 6-31g (d) level. From this β_{total}, a scalar quantity can be computed as

112   reported earlier[27, 54, 55] from the X, Y and Z components of β using equation (1).

113   $\beta_{tot} = (\beta^2_x + \beta^2_y + \beta^2_z)^{1/2}$ ....(1)

114   Where

115   $\beta^2_x = (\beta_{xxx} + \beta_{xyy} + \beta_{xzz})^2$

116   $\beta^2_y = (\beta_{yyy} + \beta_{yzz} + \beta_{yxx})^2$

117   $\beta^2_z = (\beta_{zzz} + \beta_{zxx} + \beta_{zyy})^2$

118   Time dependent density functional theory (TDDFT) has been employed

119   here to calculate the excitation energy, absorption wavelength, oscillator

120   strength on the ground state optimized geometries at 6-31g (d) level[56]. Peter

121   Bauerle *et al*. have reported the absorption spectra in dichloromethane (DCM)

122   medium for VCTO **1, 2, 3** and TDDFT calculations have been performed at

123   M062X level in the same medium. Polarizable Continuum Model (PCM) has

124   been used to find the excitation energy in the solvent medium[57]. The ionization

125   potential (IP) and electron affinity (EA) have been calculated according to

126   Koopman's theorem[58]. Further NBO analysis[59-61] has been done at B3LYP/6-

127   31g (d) level to find the most stable ground state interactions in these molecules.

128   All calculations have been carried out using the Gaussian 03 and 09 suites of

129   programs[62].

3. RESULTS AND DISCUSSION

In the present study, a total of 17 asymmetric VCTOs including three (VCTO1, VCTO2 & VCTO3) experimentally reported have been considered (**figure 1**) and they are taken as reference for validation. The chosen candidates fall into four categories, first (**VCTO1**) being the 5 alternate thiophene ring having methyl groups at 1st and 5th ring. The second category (**VCTO2**) of oligomer is taken in such a way that, it has no substitution on 5 thiophene rings, and this can be used to check effects of methyl substitution. The third category (**VCTO3**) have only 1 thiophene ring and this can be used to analyze the effect of π conjugation, with increase in thiophene rings. VCTO4 type candidates have been constructed using $-N(CH_3)_2$ as donor group.   Especially VCTO4ew (electron withdrawing group) and VCTO4er (electron releasing group) has been designed to check the contribution of electron withdrawing group and electron releasing groups towards their optoelectronic properties. This may offer a valuable clue to design more efficient newer molecules. All the three parent molecules (VCTO1, VCTO2 & VCTO3) have four -CN groups (**figure 1**) attached on either side of their vinyl moiety. Diverse structural features of these VCTOs prompted us to study how various substitutions alter the photo-physical properties of these VCTOs. Therefore, fourteen new VCTO derivatives have been designed with various substitutions as shown in **figure 1** where '**a**' represents -CN substitution **b** & **c** denotes $-NO_2$ and -COOH substitutions

151 respectively. The parent molecules do not have electron push-pull character as

152 both the sides have -CN groups; it would be interesting to substitute electron

153 donor group at one end of the molecule and examine its push-pull character. In

154 the literature dimethyl amine[54] is found to act as a good donor group and the

155 new molecules have been designed [**Figure 1**].

156 **3.1 Ground state geometries:**

157 The optimized ground state geometries of VCTOs are given in **SIF1**

158 (Supporting Information Figure 1).The important geometrical parameters are

159 listed in **table SIT1.** The computed and experimental bond parameters are in

160 good agreement. For instance, C-S bond length in VCTO3 is1.745Å and the

161 calculated value is 1.744Å, C=C bond length is 1.366Å whereas calculated C=C

162 bond length is 1.370Å which emphasize the reliability of choice of B3LYP here.

163 To understand the delocalization of π-electrons, computed bond parameters are

164 presented in **figure 2**. From the **figure 2**, it is observed that C-C, C-S, C-N are

165 all well within their single and double bond limits respectively. This indicates

166 the presence of extended π conjugation in these VCTOs. The C-C-C angle

167 between each thiophene rings varies from 124-131º. The twist angle for all

168 VCTOs lies from 153-179º. After validating the DFT method, the role of

169 electron withdrawing and releasing groups on bond parameters were analysed.

170 For example, in VCTO4ew, where there is no electron releasing group, the

171 vinylic $C_{32}=C_{39}$ bond length is 1.34 Å meanwhile, vinylic $C_{10}=C_{11}$ near the

172 electron withdrawing group experiences an elongation to 1.37Å. Moreover, in

173   VCTO4er, the same vinylic carbon near electron releasing group displayed an

174   extended bond length of 1.37Å and $C_{10}=C_{11}$ near the pull group showed bond

175   length of 1.34 Å. This shows that when the vinylic carbon is substituted by

176   electron withdrawing and electron releasing groups, the bond length was

177   stretched considerably which resulted in single and double bond character and

178   make extended conjugation in VCTOs.

179   **3.2 Frontier Molecular analysis:**

180   The characterization of chemical reactivity and kinetic stability of a

181   molecule could be made using Frontier Molecular Orbital (FMO) analysis[54, 63,

182   64]. Highest Occupied Molecular Orbital (HOMO), Lowest Unoccupied

183   Molecular Orbital (LUMO) and HOMO-LUMO energy gap gives qualitative

184   information about charge transfer interaction that occurs within a molecule[27, 54,

185   63, 64]. In order to predict the optical and electronic properties of these VCTOs,

186   the HOMO/LUMO levels were calculated and listed in supporting information

187   (**SIT2**) and shown in **figure 3**. It is well known that the electron and hole

188   transport materials should have suitable HOMO/LUMO levels in order to

189   transport electron and hole from the respective electrodes into the emitting layer

190   of OLED. Thereby controlling the HOMO and LUMO levels resulted in

191   molecules with desirable charge transport properties.

192   HOMOs are observed in the range of -7.11eV to -4.31eV and LUMOs in

193   the range of -4.08eV to -1.57eV (**Figure 3**). The calculated band gap for the

194   reported VCTOs (VCTO 1, 2 & 3) are 2.32eV, 2.23eV and3.03eV respectively.

195 It is important to note that VCTO1 (R= -CH$_3$) has 0.09eV higher than VCTO2

196 (R=H). This shows that methyl substitution has minimum contribution towards

197 the FMOs. Out of 14 designed VCTOs, six VCTOs are found to have band gap

198 lower than that of VCTO2 (2.23eV). From the figure 3, it is clear that

199 VCTO4b has lowest band gap (1.50eV) whereas the VCTO3c shows largest

200 band gap (3.16eV). In VCTO1 group, VCTO1b is found to show 0.24eV lower

201 than VCTO1. It is interesting to see that though VCTO1c has higher HOMO (-

202 4.63eV), still it shows largest band gap due to its higher LUMO (2.20eV). Thus

203 the increasing order of band gap in this VCTO1 group can be listed as VCTO1b

204 < VCTO1 < VCTO1a < VCTO1c. The HOMO of VCTO2 group of molecules

205 lie over a range of -5.64eV to -4.86eV. The HOMO-LOMO energy gap of

206 VCTO2c is found to be maximum (2.42eV) and is minimum (2.15eV) for

207 VCTO2b. Four out of five molecules (VCTO4a, 4b, 4c & 4ew) in VCTO4

208 group is found to show reduced band gap than VCTO2. VCTO4er is found to

209 have higher band gap 2.51eV than the rest in VCTO4 group. This shows that the

210 acceptor group is very important in the band gap reduction in these molecules.

211 VCTO4b and VCTO1b differ only one donor and acceptor group (-NO$_2$ & -

212 N(CH$_3$)$_2$ group and this additional donor and acceptor group in VCTO4b plays a

213 major role in bringing down the HOMO-LUMO energy gap from 2.08eV to

214 1.50eV. When comparing VCTO1a and VCTO4a, HOMO is elevated to -4.49

215 from -4.67 while LUMO lowers to -2.78eV from 2.31eV. it is evident that the

216 additional donor and acceptor groups is playing vital role in altering the FMOs.

217   By looking at the structure of VCTO4s (figure 1), this group can be classified

218   into three categories; VCTO4er (donor alone), VCTOew (acceptor alone) and

219   VCTO4a, 4b & 4c (Donor-π-Acceptor). The increasing band gap order in

220   VCTO4s is as follows, VCTO4b < VCTO4a < VCTO4c < VCTOew <

221   VCTO4er. This shows that Donor-π-Acceptor molecules are superior to

222   Acceptor-π-Acceptor (VCTO1, VCTO2 & VCTO3) type molecules.

223   The Frontier Molecular Orbitals (LUMO+1, LUMO, HOMO & HOMO-

224   1) of all 'b' molecules of VCTOs (VCTO1b, 2b, 3b & 4b) are given in figure 4.

225   The complete FMOs of all the VCTOs are deposited in SIF2-SIF5. From the

226   figure, it is clear that HOMO and LUMO of VCTO3b is evenly localized on the

227   entire molecule. This ensures the HOMO→LUMO transition in VCTO3b is due

228   to π→π* transition. In contrast to the HOMO of VCTO1b, 2b & 3b is mainly

229   localized by the donor and π-bridge units whereas LUMO is largely stabilized

230   by the acceptor groups and few thiophene units. This indicates that HOMO →

231   LUMO transition arises from intra-molecular charge transfer character (IMCT).

232   Meanwhile, the experimentally reported VCTOs (VCTO1, 2 & 3) exhibits a

233   typical π – π* transition (**SIF2-SIF4**). This shows that the introduction of

234   electron releasing group on VCTOs made HOMO→LUMO transition as IMCT.

235   This IMCT character of HOMO →LUMO transition is reflected in absorption

236   maxima (λ_{max}) which is discussed in section 3.7.

237   To gain further insights from these FMOs, energetics of the HOMOs and

238   LUMOs are analyzed using QMForge[27, 54, 64] and the results are summarized in

239   **table 1**. The whole molecule is segmented into four fragments namely,

240   thiophene rings (π-bridge), N,N-Dimethyl amine (Donor), -CN,-NO$_2$,-COOH

241   (Acceptor) & methyl groups at thiophene ring (Methyl) and their corresponding

242   compositions are computed. From the table, it is clear that both the HOMO and

243   LUMO of VCTO1 is found to get 87% & 79% from the π-bridge unit

244   respectively. Only 1% of contribution is from methyl group towards HOMO

245   and LUMO of VCTO1 and this is also reflected in the FMOs (SIF2). π-bridge

246   is contributing nearly ~50% towards HOMO & LUMO in VCTO3s and this is

247   due to lesser number of thiophene units in this group. The contribution of donor

248   in VCTO3s is the highest (~35%) among the VCTOs. The lowest band gap

249   VCTO4b gets 27% from the donor towards HOMO and its contribution is

250   reduced to less than 1% in LUMO. But contribution of acceptor unit raises

251   from 1% to 34% moving from HOMO to LUMO in VCTO4b. As expected the

252   donor contributes 24% towards HOMO in VCTO4er while acceptor contributes

253   21% towards the stabilization of LUMO in VCTOew. Invariably in all the

254   molecules, the π-bridge predominantly contributes to HOMO & LUMO (43% to

255   93%). Except VCTO3s, all the other VCTOs, the contribution of π-bridge is at

256   least twice higher than corresponding donor and acceptor. On the whole, this

257   study implies the fact that π-bridge needs to be substituted by electron releasing

258   groups to alter the HOMO while LUMO can be altered by substituting electron

259   withdrawing groups. Thus fragment analysis, sheds light on how to alter

260   HOMO and LUMO contributions by making suitable substitution on the π

261   bridge.

3.3 Dipole moment:

263   The dipole moment calculations give a clear picture of the electronic

264   charge distribution in the molecule. So it is intended to analyse and compare the

265   dipole moment (μ) in gas phase and solution phase (dichloromethane medium,

266   DCM) of the VCTOs considered here **(table 2)**. The highest dipole moment (μ

267   in Debye) in gas phase is observed for VCTO4b (16.94D) VCTO3 & VCTO3c

268   who have wide band gap have lower dipolemoment (4.41D). Table 2 shows that

269   VCTOew and VCTOer are found to show large (6.63D) difference in

270   dipolemoment. This shows that electron withdrawing group enhances the

271   dipolemoment of VCTOs. VCTO2 has dipolemoment of 9.37D which is twice

272   as that of VCTO3 (4.41D). This is due to the presence of long π-bridge

273   (thiophene units) in VCTO2. It is noteworthy that solvation increases the

274   dipolemoment upto 7.11D (**Table 2**). Solvation has least effect (0.8D) on the

275   dipolemoment of VCTO2c whereas difference of 7.11D is observed for

276   VCTO3 while moving from gas to solution phase. In general, the dipolemoment

277   of reference molecules (VCTO1, 2 & 3) are largely affected by solvation. But

278   the dipolemoment of all the carboxylic acid derivates (VCTO1c, 2c, 3c & 4c)

279   are found to show less response (~1D) to solvation. Among the designed

280   VCTOs, highest dipolemoment of 21.20D is exhibited by VCTO4b whereas

281   only 5.39D is observed for VCTO3c. In general the calculated dipolemoments

282   are in harmony with the calculated HOMO-LUMO energy gap.

283   **3.4 NLO properties:**

284   The NLO response of whole molecule has been made by individual

285   contribution of basic molecular unit in an organic material. Study on NLO

286   activity emphasized a third rank tensor called first-order hyper polarizability

287   (β_0). It can be described by a 3x3x3 matrix. This 3D matrix with 27 components

288   can be reduced to 10 components due to kleinman symmetry[65]. It is aimed to

289   analyse and compare the electronic effects on β_0 of VCTOs and the results are

290   summarized in **table 2**.

291   The calculated β_0 of VCTO4s, follows the increasing order as VCTO4er

292   < VCTO4ew < VCTO4c < VCTO4a < VCTO4b. It is important to note that

293   there is an excellent agreement with the computed NLO response and the

294   computed band gap. For example, the lowest band gap VCTO4b is found to

295   show high hyper polarizability (3278.83esu) whereas the wide band gap

296   VCTO3c has a very low hyper polarizability of 43.69esu. It is evident from the

297   **table 2**, the first order hyper polarizability of VCTO1 & 2 are much lower than

298   their designed candidates. For instance, VCTO2 has 44.8esu and 963.55esu is

299   observed for VCTO2b. This shows that D-π-A type is better than A- π-A type

300   molecules. It is interesting to note that VCTO3s have a very low

301   hyperpolarizability values (upto ~19 esu) even after the introduction of donor or

302   acceptor. This suggests that π-conjugation is important in these systems for

303　enhanced NLO property. The relationship between band gap and hyper

304　polarizability (β_0) has been evaluated using correlation coefficient parameter

305　(R^2) by quadratic fitting equation. About 99% correlation was achieved in β_0

306　against band gap. This linear trend has shown in **figure 5**. Earlier study[66]

307　indicates, β_0 is inversely related to transition energy (ΔE). Accordingly,

308　VCTO4b, with minimum transition energy of 2.28eV showcased a highest β_0

309　value of 3278.83 X 10^{-30}esu. A higher magnitude of β_0 and dipole moment is

310　essential for pronounced NLO activity and the present study clearly illustrates

311　that the D-π-A VCTOs are the best choice of material for NLO application than

312　the electron withdrawing type of molecule.

313　**3.5 Conducting properties:**

314　　　The ability to transport charge, its injection and their balance always

315　associated with the performance of optoelectronic compounds. Therefore it is

316　essential to investigate global reactivity descriptors such as Ionization potential

317　(IP), electron affinity (EA) and exciton binding energy (E_b) to evaluate transport

318　ability of these VCTOs (**Table 3**). The IPs and EAs can be expressed through

319　HOMO and LUMO orbital energies according to Koopman's theorem[58]. It is

320　well known that in OLEDs, lower IP leads to easy injection of holes from the

321　hole transport layer (HTL) and higher EA paves the way for the easy injection

322　of electrons from electron transport layer (ETL). From table 3, it is clear that

323　the reference VCTOs (VCTO1, 2 & 3) found to show high IPs than the

324　designed VCTOs. The increasing order of IPs in reference VCTOs follows as

325 VCTO1< VCTO2< VCTO3. This shows that these VCTOs are found to have

326 poor hole transport character. But all the designed VCTOs are found to show

327 lower IPs than the reference molecules.   Among D-π-A molecules, all the

328 carboxylic acid derivatives found to have low IPs than their corresponding

329 cyano and nitro derivatives. The calculated EA values suggest that carboxylic

330 acid derivatives have lesser EA than that of designed VCTOs. This shows that

331 these carboxylic acid derivatives are good hole transport materials. It is

332 important to note that VCTO4ew has high EA value than that of VCTO4er. This

333 shows that EW group improves the electron transporting character while

334 VCTOer has the least IP value among all the VCTOs suggesting that ER group

335 increases the hole transport properties. Thus the donors and acceptors alter the

336 IPs and EAs significantly.

337   Exciton binding energy (E_b) is used to estimate the energy conversion

338 efficiency of a molecule. Hence the exciton binding energy has been calculated

339 as reported earlier[67]. The E_b values reported in table 3 suggests that the

340 reference VCTOs have nearly the same value, -0.10, -0.10, -0.11eV higher than

341 that of designed VCTOs. This tells that D-π-A type molecules found to have

342 better energy conversion efficiencies than A- π-A type molecules. The energy

343 conversion efficiencies are in good agreement with the calculated FMO

344 energies. For instance the low band gap VCTO4b has the least E_b of -0.78eV

345 and the wide band gap VCTO3s have higher E_b. This shows lower the HOMO-

346 LUMO gap, lower the E_b and higher the energy conversion efficiency.

347 **3.6 Charge analysis:**

348   The NBO charges help to identify distribution of charge in the

349 molecule[61]. Moreover the charge transport ability of a molecule depends on the

350 magnitude of charge on the different segments of a molecule. Therefore NBO

351 charges have been calculated on donor and acceptor moieties of VCTOs (**SIF6**)

352 and the results are shown in figure 6 & **SIT3**. Before going into the discussion,

353 it is important to recall that a good charge transport molecule should have more

354 positive charge on donor moiety which can be readily available for donation.

355 Similarly the acceptor moiety should accept the donated charges and become

356 more negative. This facilitates the transportation of charge throughout the

357 molecule. From the **Figure 6,** it is clear that all the donors have more positive

358 charges. Especially VCTO3a has the largest (+0.336) among all the VCTOs. As

359 expected, the acceptors have more negative charges (from -0.151 to -0.692).

360 Especially D-π-A molecules have high positive and negative charges on either

361 ends. This suggests that charge is readily moved from donor to acceptor thereby

362 making these molecules to have a high charge transport character. At the same

363 time, VCTO4er and VCTO4ew has positive and negative charges on either

364 ends respectively. This shows that these two molecules have relatively less

365 charge transport character than other VCTO4s.

366

367

368

369   **3.7 Electronic absorption spectra**

370   For a molecule to display good NLO property it has to show good

371   absorption and emission properties[54]. TDDFT calculations have been performed

372   to compute excited state properties[68-71] and to get electronic vertical singlet

373   excitation energies in gas phase. In the literature, different functionals have

374   been reported for the calculation of absorption spectra of organic molecules[72-74].

375   Therefore, it is essential to use appropriate functional that gives accurate

376   predictions of absorption spectra. In order to identify the more reliable method

377   to predict the absorption spectra of these VCTO derivatives, different

378   functionals (B3LYP, B1LYP, CAM-B3LYP, PBE and MO62X) have been

379   tested by comparing with the available experimental results (SIT4). From the

380   computed results, it is clear that the λ_{max} estimated at MO62X/6-31g(d) level

381   agrees well with the experimentally observed absorption maxima (see table

382   SIT4). Therefore the M062X functional is used for TDDFT calculations

383   throughout the study.

384   The calculated vertical transition energies (ΔE), oscillator strength (f),

385   transition assignments and their percentage of various configurations to the

386   excitations are summarized in **table 4**. The λ_{max} value displayed in **table 4** is the

387   most intense band that can be assigned to $S_0 \rightarrow S_1$ transition. The computed

388   absorption maxima for all these VCTOs lie in the range of 360-545nm which

389   implies that their emission will be at still higher wavelengths making them

390   suitable for optoelectronic applications. From the table it is clear that the

391 absorption of these systems can be shifted to longer or shorter wavelengths by

392 by substituting ER and EW groups in the skeleton. As expected, lowest band

393 gap VCTO4b has the longest wavelength absorption (545nm). This arises due to

394 64% & 19% of contributions from HOMO→LUMO and HOMO-1→LUMO

395 respectively.   It is evident from the data presented in table 4 that VCTO3s have

396 predominant HOMO→ LUMO contributions (>97%) for their intense band and

397 are due to π-π* transitions. But other VCTOs (VCTO1, 2 & 4 group of

398 molecules) found to show both π-π* transitions and intramolecular charge

399 transfer character. In VCTO2s, all the molecules found to have absorption

400 wavelength of more than 400nm with VCTO2b & VCTO2 as highest and

401 lowest the λ_{max} respectively. The substituent EW groups has a large influence on

402 the absorption spectrum than ER group. For instance, VCTO4ew has the λ_{max} at

403 476 nm VCTO4er λ_{max} has it at 444nm.

404

405 **3.8 Effect of solvent on UV absorption spectra:**

406   The solvent effect on the absorption spectrum of VCTOs is investigated

407 by performing PCM calculations with dichloromethane as solvent. The PCM

408 calculations have been identified as the most successful model for describing

409 solvent effect in DFT and TDDFT calculations.[75, 76]. The results of the

410 calculations for ten lowest lying excited states were calculated on VCTOs and

411 their important excitation wavelength along with their oscillator strength are

412 shown in **table 5**. It is interesting to note that the calculated absorption maxima

413   of experimentally reported VCTOs are in good agreement with the experimental

414   report[23]. The measured results show that the molecules show a shift in the

415   absorption spectra upon solvation (15-117nm). Especially VCTO2 is found to

416   show a shift from 415nm to 532nm. But solvation has little effect on VCTO2a

417   & 2c where they have a shift of only 15nm upon solvation. The

418   HOMO→LUMO configurations of VCTO1 contributes 83% to absorption at

419   513nm which is 109nm higher than that of in gas phase. The transition arising

420   from $S_0 \rightarrow S_1$ is the most intense band in all VCTOs. All the VCTOs found to

421   show positive solvatochromism yet the overall trend in the absorption remains

422   the same in both gas and solvent phases. Light Harvesting Efficiency (LHE),

423   another interesting property, is calculated and results are given in table 5. It is

424   important to note that the LHE varies from 0.85 to 0.99 which is closer to

425   1.This shows that all the VCTOs are found to have good light harvesting

426   character.

427

428   **3.9 NBO analysis:**

429   The NBO analysis is a powerful tool that reveals the nature of electronic

430   interactions and of electronic structure properties, which are solely responsible

431   in deciding the chemical entity of the molecules[27, 54, 61]. The properties are Lewis

432   donor, non Lewis acceptor, orbital energy, % electron density (%ED),

433   stabilization energy (E2) and the energy splitting (E_j-E_i) between Lewis and non

434   Lewis structures. The energy gap between Lewis bonding orbital and non Lewis

anti bonding orbital decides the feasibility of interaction between filled donor

and acceptor moieties. The % ED of the Lewis donor and non Lewis acceptor

involved in hyper conjugative interaction, orbital energy, and stabilization

energy has been computed using second order perturbation approach[61] at the

B3LYP/ 6-31g (d) level   and the results are displayed in **table 6**. The

interactions between occupied and unoccupied levels of VCTO1s are depicted

in **figure 7** and the same for other systems are collected in **SIF7-SIF10**.

As seen from the table, the stabilization energy is high for VCTO (1b, 2b,

3b and 4c) and increases in the following order VCTO3b > VCTO4b >

VCTO1b > VCTO2b. The calculated % of electron density distribution (ED) on

non-Lewis moieties in VCTO2a is 48.44 (C_{13})-51.56 (C_{14}). Though several

types of electronic interactions are present between occupied and unoccupied

levels the most dominant stabilization comes from n$\rightarrow$π* and π$\rightarrow$π* in VCTOs.

The lone pair (LP) of N, S and O donate electrons to anti bonding π^*_{C-C}, π^*_{C-O},

π^*_{N-O} orbitals. The second order stabilization (39.86 kJ/mol) in VCTO1a is due

to lone pair localized on N_{54} and $\pi^*_{C11-C18}$. The computed second order

perturbation analysis conducted on VCTOs, clearly conveys the presence of

most stable orbital overlap between donor and acceptor fragments. Especially

all the nitro derivative VCTOs are found to show large second order

perturbation interactions than that of other VCTOs (Table 6).

The present studies show that 9 out of 17 VCTOs have promising

optoelectronic properties than their corresponding reference VCTO. Among the

21

457   designed VCTOs, VCTO4b is found to show excellent optoelectronic properties

458   with low band gap (1.50 eV), high wavelength of absorption (576 nm),

459   displayed   a   remarkable   NLO   property

460   (β_0=3278.83 esu), and would be a best bet for future optoelectornic applications.

461

462   **4.0 Conclusions**

463   Totally 17 VCTOs, 3 of them reported by Peter Baurele *et al* and 14

464   newly designed here, have been studied using DFT/TDDFT methods, in order

465   to sort candidates with best optoelectronic properties. Computed results show

466   that experimentally synthesized, acceptor- acceptor type VCTOs have low band

467   gap and the designed candidates have high wavelength absorption. VCTO4b is

468   found to be the best candidate with low band gap whereas VCTO3c is to be the

469   poor candidate. Further VCTO4b possesses high wavelength of absorption, high

470   β_0 value and high dipole moment. HOMO-LUMO analysis reveals that -NO$_2$

471   group is playing a major role in stabilizing the LUMO compared to other

472   acceptors (-CN & -COOH). The reference VCTOs showed $\pi\rightarrow\pi$ * transition

473   while, designed VCTOs displayed n$\rightarrow\pi$ * transition with IMCT character. The

474   exciton binding energy was less for designed VCTOs and exhibits a huge light

475   harvesting efficiency than the reference molecules. The electronic stabilization

476   of the molecule was understood by NBO analysis. Further this study reveals that

477   the reference VCTOs can be better electron transport material while designed

478   VCTOs are hole transport material, which leads to the   point that donor-

479 acceptor substitution in the skeleton can convert a electron transport material

480 into hole transport material. Overall, the present study rationalizes the optical

481 property of VCTO can be tuned by suitable substitution to achieve remarkable

482 optoelectronic properties.

483 **5.0 Acknowledgement**

490 **6.0 Supporting Information:**

491 XYZ coordinates, bond parameters, NBO analysis, HOMO-LUMO energies are

492 available in the supporting information.

493

494

495

496

497

498

499

7.0 References

1. C.-J. Huang, J.-C. Ke, W.-R. Chen, T.-H. Meen and C.-F. Yang, *Solar Ener. Mater. Solar Cells*, 2011, **95**, 3460-3464.
2. Y. Li, T. Pullerits, M. Zhao and M. Sun, *J. Phys. Chem. C*, 2011, **115**, 21865-21873.
3. G. Paramaguru, R. V. Solomon, S. Jagadeeswari, P. Venuvanalingam and R. Renganathan, *Euro. J. Org. Chem.*, 2014, **2014**, 753-766.
4. E. Sengupta, A. L. Domanski, S. A. Weber, M. B. Untch, H.-J. r. Butt, T. Sauermann, H. J. Egelhaaf and R. d. Berger, *J. Phys. Chem. C*, 2011, **115**, 19994-20001.
5. H. Tachikawa and H. Kawabata, *J. Organomet. Chem.*, 2012, **720**, 60-65.
6. G. Velmurugan, B. K. Ramamoorthi and P. Venuvanalingam, *Phys. Chem. Chem. Phys.*, 2014, **16**, 21157-21171.
7. Y. Zhou, J. W. Shim, C. Fuentes-Hernandez, T. M. Khan and B. Kippelen, *Thin Solid Films*, 2014, **554**, 54-57.
8. H. Furukawa, K. E. Cordova, M. O'Keeffe and O. M. Yaghi, *Science*, 2013, **341**, 1230444.
9. H. Furukawa, N. Ko, Y. B. Go, N. Aratani, S. B. Choi, E. Choi, A. Ö. Yazaydin, R. Q. Snurr, M. O'Keeffe and J. Kim, *Science*, 2010, **329**, 424-428.
10. F. J. Uribe-Romo, J. R. Hunt, H. Furukawa, C. Klöck, M. O'Keeffe and O. M. Yaghi, *J. Am. Chem. Soc.*, 2009, **131**, 4570-4571.
11. H. M. El-Kaderi, J. R. Hunt, J. L. Mendoza-Cortés, A. P. Côté, R. E. Taylor, M. O'Keeffe and O. M. Yaghi, *Science*, 2007, **316**, 268-272.
12. A. P. Cote, A. I. Benin, N. W. Ockwig, M. O'Keeffe, A. J. Matzger and O. M. Yaghi, *Science*, 2005, **310**, 1166-1170.
13. Z. Hu, C.-a. Tao, F. Wang, X. Zou and J. Wang, *Journal of Materials Chemistry C*, 2015, **3**, 211-216.
14. C. H. Hendon, D. Tiana, M. Fontecave, C. m. Sanchez, L. D'arras, C. Sassoye, L. Rozes, C. Mellot-Draznieks and A. Walsh, *J. Am. Chem. Soc.*, 2013, **135**, 10942-10945.
15. Y. Zhou, Z. Wang, P. Yang, X. Zu and F. Gao, *J. Mater. Chem.*, 2012, **22**, 16964-16970.
16. L.-M. Yang and R. Pushpa, *Journal of Materials Chemistry C*, 2014, **2**, 2404-2416.
17. E. Klontzas, E. Tylianakis and G. E. Froudakis, *Nano letters*, 2010, **10**, 452-454.
18. H. Zhang, *Bulletin of the American Physical Society*, 2014, **59**.
19. S.-Y. Ding and W. Wang, *Chemical Society Reviews*, 2013, **42**, 548-568.
20. M. Klimakow, P. Klobes, K. Rademann and F. Emmerling, *Microporous and Mesoporous Materials*, 2012, **154**, 113-118.
21. C. K. Brozek and M. Dincă, *J. Am. Chem. Soc.*, 2013, **135**, 12886-12891.
22. N. Nijem, H. Wu, P. Canepa, A. Marti, K. J. Balkus Jr, T. Thonhauser, J. Li and Y. J. Chabal, *J. Am. Chem. Soc.*, 2012, **134**, 15201-15204.
23. R. Fitzner, E. Mena-Osteritz, A. Mishra, G. Schulz, E. Reinold, M. Weil, C. Körner, H. Ziehlke, C. Elschner, K. Leo, M. Riede, M. Pfeiffer, C. Uhrich and P. Bäuerle, *J. Am. Chem. Soc.*, 2012, **134**, 11064-11067.
24. L. Dou, J. You, J. Yang, C.-C. Chen, Y. He, S. Murase, T. Moriarty, K. Emery, G. Li and Y. Yang, *Nature Photon.*, 2012, **6**, 180-185.
25. A. Diaz, K. K. Kanazawa and G. P. Gardini, *J. Chem. Soc. Chem. Commun.*, 1979, 635-636.
26. J. Roncali, *Chem. Rev.*, 1992, **92**, 711-738.
27. R. V. Solomon, R. Jagadeesan, S. A. Vedha and P. Venuvanalingam, *Dyes&Pigments*, 2014, **100**, 261-268.
28. G. Tourillon and F. Garnier, *J. Electrochem. Soc.*, 1983, **130**, 2042-2044.
29. R. J. Waltman, J. Bargon and A. Diaz, *J. Phys. Chem.*, 1983, **87**, 1459-1463.
30. S. Glenis, M. Benz, E. LeGoff, J. Schindler, C. Kannewurf and M. Kanatzidis, *J. Am. Chem. Soc.*, 1993, **115**, 12519-12525.
31. E. Maarouf, D. Billaud and E. Hannecart, *Mater. Res. Bullet.*, 1994, **29**, 637-643.

550 32. T.-Y. Chu, S. Alem, P. G. Verly, S. Wakim, J. Lu, Y. Tao, S. Beaupré, M. Leclerc, F. Bélanger and
551   D. Désilets, *Appl. Phys. Lett.*, 2009, **95**, 063304.
552 33. M. Delamar, P.-C. Lacaze, J.-Y. Dumousseau and J.-E. Dubois, *Electrochimica Acta*, 1982, **27**,
553   61-65.
554 34. J. Rault-Berthelot, L. Angely, J. Delaunay and J. Simonet, *New J. Chem.*, 1987, **11**, 487-494.
555 35. A. Bongini, G. Barbarella, L. Favaretto, G. Sotgiu, M. Zambianchi and D. Casarini,
556   *Tetrahedron*, 2002, **58**, 10151-10158.
557 36. J. Brédas, J. Cornil, F. Meyers, D. Beljonne, T. Skotheim, R. Elsenbaumer and J. Reynolds,
558   *Handbook of conducting polymers*, 1998, 1-26.
559 37. D. Fichou, *Handbook of oligo-and polythiophenes*, John Wiley & Sons, 2008.
560 38. F. Garnier, *Acc. Chem. Res.*, 1999, **32**, 209-215.
561 39. K. Mullen and G. Wegner, *Electronic materials*, Wiley, 2008.
562 40. J. Rogers and H. Katz, *J. Mater. Chem.*, 1999, **9**, 1895-1904.
563 41. A. Alberti, L. Favaretto, G. Seconi and G. F. Pedulli, *J. Chem. Soc., Perkin Trans. 2*, 1990, 931-
564   935.
565 42. Y. Cao, D. Guo, M. Pang and R. Qian, *Syn. Mat.*, 1987, **18**, 189-194.
566 43. J. V. Caspar, V. Ramamurthy and D. R. Corbin, *J. Am. Chem. Soc.*, 1991, **113**, 600-610.
567 44. D. Fichou, G. Horowitz and F. Garnier, *Syn. Mat.*, 1990, **39**, 125-131.
568 45. H. Fujimoto, U. Nagashima, H. Inokuchi, K. Seki, Y. Cao, H. Nakahara, J. Nakayama, M.
569   Hoshino and K. Fukuda, *J. Chem. Phys.*, 1990, **92**, 4077-4092.
570 46. D. Jones, M. Guerra, L. Favaretto, A. Modelli, M. Fabrizio and G. Distefano, *J. Phys. Chem.*,
571   1990, **94**, 5761-5766.
572 47. G. Zerbi, B. Chierichetti and O. Ingänas, *J. Chem. Phys.*, 1991, **94**, 4637-4645.
573 48. U. Schoeler, K. Tews and H. Kuhn, *J. Chem. Phys.*, 1974, **61**, 5009-5016.
574 49. A. Mishra and P. Bäuerle, *Angew. Chem. Int. Ed.*, 2012, **51**, 2020-2067.
575 50. A. D. Becke, *J. Chem. Phys.*, 1993, **98**, 5648-5652.
576 51. C. Lee, W. Yang and R. G. Parr, *Phys. Rev. B*, 1988, **37**, 785.
577 52. L. A. Curtiss, K. Raghavachari, P. C. Redfern and J. A. Pople, *Chem. Phys. Lett.*, 1997, **270**, 419-
578   426.
579 53. E. Kleinpeter and B. A. Stamboliyska, *J. Org. Chem.*, 2008, **73**, 8250-8255.
580 54. R. V. Solomon, P. Veerapandian, S. A. Vedha and P. Venuvanalingam, *J. Phys. Chem. A*, 2012,
581   **116**, 4667-4677.
582 55. K. S. Thanthiriwatte and K. Nalin de Silva, *J. Mol. Struct. THEOCHEM*, 2002, **617**, 169-175.
583 56. R. Improta, V. Barone, G. Scalmani and M. J. Frisch, *J. Chem. Phys.*, 2006, **125**, 054103.
584 57. S. Miertuš, E. Scrocco and J. Tomasi, *Chem. Phys.*, 1981, **55**, 117-129.
585 58. T. Koopmans, *Physica*, 1934, **1**, 104-113.
586 59. E. Glendening, A. Reed, J. Carpenter and F. Weinhold, *NBO version*, 1998, **3**.
587 60. A. E. Reed, L. A. Curtiss and F. Weinhold, *Chem. Rev.*, 1988, **88**, 899-926.
588 61. F. Weinhold, *J. Comput. Chem.*, 2012, **33**, 2363-2379.
589 62. M. J. T. Frisch, G. W.; Schlegel, H. B.; Scuseria, G. E.; Robb, M. A.; Cheeseman, J. R.; Scalmani,
590   G.; Barone, V.; Mennucci, B.; Petersson, G. A.; Nakatsuji, H.; Caricato, M.; Li, X.; Hratchian, H.
591   P.; Izmaylov, A. F.; Bloino, J.; Zheng, G.; Sonnenberg, J. L.; Hada, M.; Ehara, M.; Toyota, K.;
592   Fukuda, R.; Hasegawa, J.; Ishida, M.; Nakajima, T.; Honda, Y.; Kitao, O.; Nakai, H.; Vreven, T.;
593   Montgomery, Jr., J. A.; Peralta, J. E.; Ogliaro, F.; Bearpark, M.; Heyd, J. J.; Brothers, E.; Kudin,
594   K. N.; Staroverov, V. N.; Kobayashi, R.; Normand, J.; Raghavachari, K.; Rendell, A.; Burant, J.
595   C.; Iyengar, S. S.; Tomasi, J.; Cossi, M.; Rega, N.; Millam, N. J.; Klene, M.; Knox, J. E.; Cross, J.
596   B.; Bakken, V.; Adamo, C.; Jaramillo, J.; Gomperts, R.; Stratmann, R. E.; Yazyev, O.; Austin, A.
597   J.; Cammi, R.; Pomelli, C.; Ochterski, J. W.; Martin, R. L.; Morokuma, K.; Zakrzewski, V. G.;
598   Voth, G. A.; Salvador, P.; Dannenberg, J. J.; Dapprich, S.; Daniels, A. D.; Farkas, Ö.; Foresman,
599   J. B.; Ortiz, J. V.; Cioslowski, J.; Fox, D. J. Gaussian 09, Revision B.01, Gaussian, Inc.,
600   Wallingford CT, 2009.

601   63.   R. G. Pearson, in *Chemical hardness*, Springer, 1993, pp. 1-10.
602   64.   R. V. Solomon, A. P. Bella, S. A. Vedha and P. Venuvanalingam, *Phys. Chem. Chem. Phys.*,
603   2012, **14**, 14229-14237.
604   65.   D. Kleinman, *Phys. Rev.*, 1962, **126**, 1977.
605   66.   M. R. S. A. Janjua, M. U. Khan, B. Bashir, M. A. Iqbal, Y. Song, S. A. R. Naqvi and Z. A. Khan,
606   *Comput. Theor. Chem.*, 2012, **994**, 34-40.
607   67.   R. Nithya and K. Senthilkumar, *Phys. Chem. Chem. Phys.*, 2014, **16**, 21496-21505.
608   68.   C. M. Aikens, S. Li and G. C. Schatz, *J. Phys. Chem. C*, 2008, **112**, 11272-11279.
609   69.   E. Gross and W. Kohn, *Adv. Quant. Chem.*, 1990, **21**, 255-291.
610   70.   J. Kulhánek, F. Bures, A. Wojciechowski, M. Makowska-Janusik, E. Gondek and I. Kityk, *J.*
611   *Phys. Chem. A*, 2010, **114**, 9440-9446.
612   71.   M. Makowska-Janusik, I. Kityk, J. Kulhanek and F. Bures, *J. Phys. Chem. A*, 2011, **115**, 12251-
613   12258.
614   72.   P. J. Aittala, O. Cramariuc, T. I. Hukka, M. Vasilescu, R. Bandula and H. Lemmetyinen, *J. Phys.*
615   *Chem. A*, 2010, **114**, 7094-7101.
616   73.   M. J. G. Peach, C. R. Le Sueur, K. Ruud, M. Guillaume and D. J. Tozer, *Phys. Chem. Chem.*
617   *Phys.*, 2009, **11**, 4465-4470.
618   74.   I. Petsalakis, D. Georgiadou, M. Vasilopoulou, G. Pistolis, D. Dimotikali, P. Argitis and G.
619   Theodorakopoulos, *J. Phys. Chem. A*, 2010, **114**, 5580-5587.
620   75.   A. Pedone, J. Bloino, S. Monti, G. Prampolini and V. Barone, *Phys. Chem. Chem. Phys.*, 2009,
621   **12**, 1000-1006.
622   76.   V. Barone, J. Bloino, S. Monti, A. Pedone and G. Prampolini, *Phys. Chem. Chem. Phys.*, 2010,
623   **12**, 10550-10561.

624

625

626

627

628

629

630

631

632

633

634

635

636

637 **Figure captions;**

638 Figure 1 Structure of the designed and reference VCTO molecules.

639 Figure 2 Depiction of delocalization of electron in VCTOs from calculated C-C, C-N, C-S

640 bond length.

641 Figure 3 Frontier molecular orbital energy level diagram of designed VCTOs.

642 Figure 4 Frontier molecular orbitals of nitro derivatives of VCTOs.

643 Figure 5 Relationship between band gap and hyper polarizability (β_0) from correlation

644 coefficient analysis.

645 Figure 6 NBO charges of VCTOs calculated on donor & acceptor moieties.

646 Figure 7 Illustration of second order perturbation interactions in VCTO1s from NBO

647 analysis.

648

649

650

651

652

653

654

655

656

657

658

659

660

661

662

663

664

665

666

667

668

669
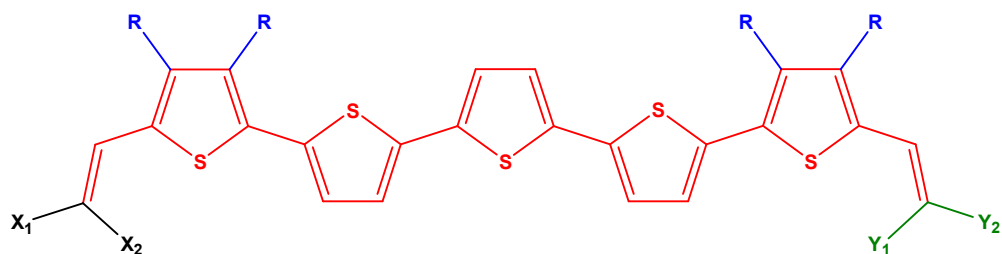
670

VCTO1   : R=CH_3 ; X_1,X_2 & Y_1,Y_2=CN
VCTO1a : R=CH_3 ; X_1=CN ; Y_1=$N(CH_3)_2$; X_2 & Y_2=H
VCTO1b : R=CH_3 ; X_1=NO_2 ; Y_1=$N(CH_3)_2$; X_2 & Y_2=H
VCTO1c : R=CH_3 ; X_1=COOH ; Y_1=$N(CH_3)_2$; X_2 & Y_2=H
VCTO2   : R=H   ; X_1,X_2 & Y_1,Y_2=CN
VCTO2a : R=H   ; X_1=CN ; Y_1=$N(CH_3)_2$; X_2 & Y_2=H
VCTO2b : R=H   ; X_1=NO_2 ; Y_1=$N(CH_3)_2$; X_2 & Y_2=H
VCTO2c : R=H   ; X_1=COOH ; Y_1=$N(CH_3)_2$; X_2 & Y_2=H
VCTO4ew : R=CH_3 ; X_1,X_2=CN & Y_1,Y_2=H
VCTO4a : R=CH_3 ; X_1,X_2=CN ; Y_1,Y_2=$N(CH_3)_2$
VCTO4b : R=CH_3 ; X_1,X_2=NO_2 ; Y_1,Y_2=$N(CH_3)_2$
VCTO4c : R=CH_3 ; X_1,X_2=COOH ; Y_1,Y_2=$N(CH_3)_2$
VCTO4er : R=CH_3 ; X_1,X_2=H ; Y_1,Y_2=$N(CH_3)_2$;
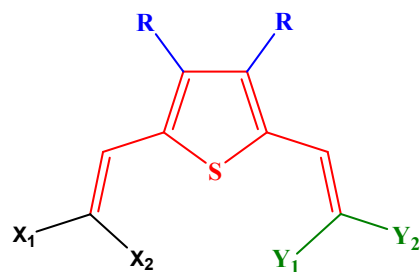
VCTO3 : R=H ; X_1,X_2 & Y_1,Y_2=CN
VCTO3a : R=H ; X_1=CN ; Y_1=$N(CH_3)_2$; X_2 & Y_2=H
VCTO3b : R=H ; X_1=NO_2 ; Y_1=$N(CH_3)_2$; X_2 & Y_2=H
VCTO3c : R=H ; X_1=COOH ; Y_1=$N(CH_3)_2$; X_2 & Y_2=H

Figure 1

28
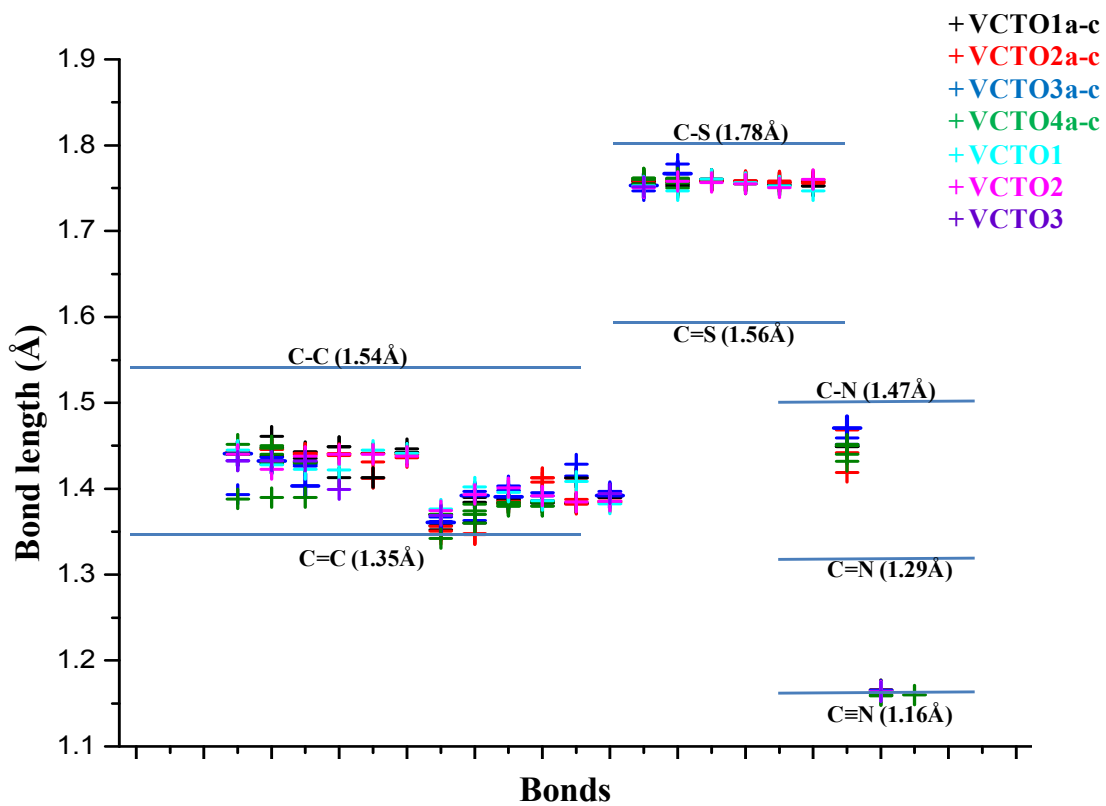
Figure 2

729

730

731

732

733

734

735

736

737

738

739

740

741

742

743

744

745

746

747

748

749

750

751

752

753

754

755

756

757

758 **Figure 3**

759

760

761

762
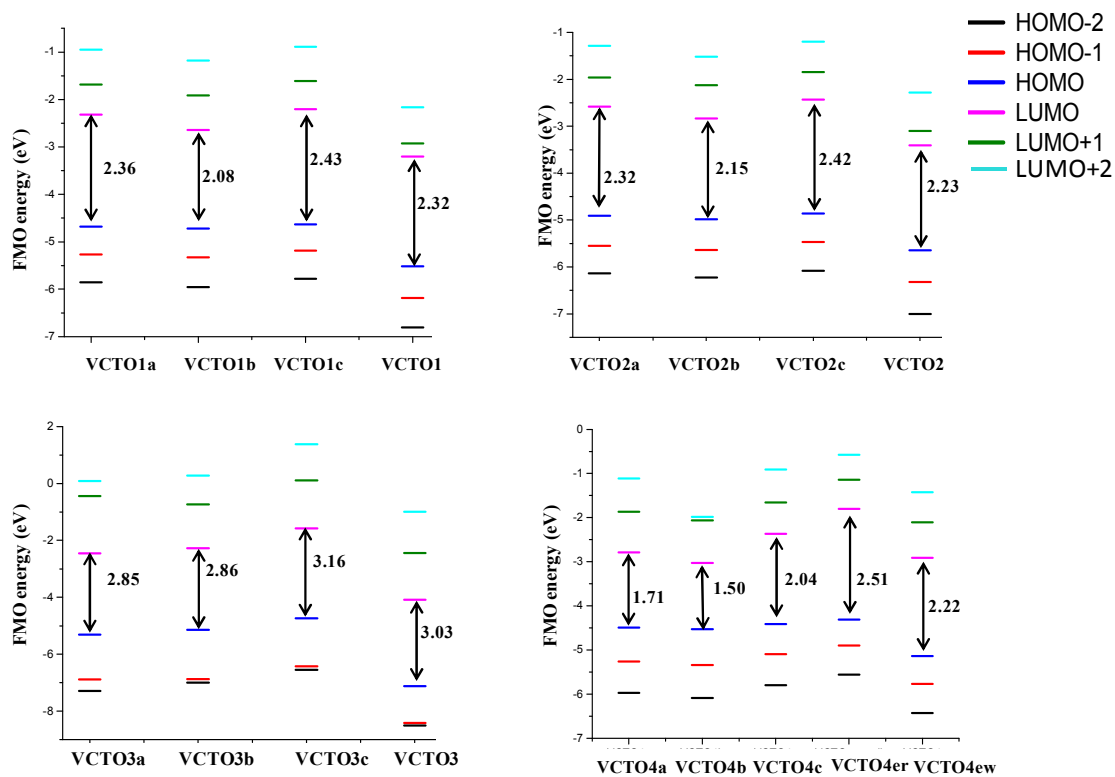
763

764

765

766

767

768

769

770

771   LUMO+1

772

773

774   LUMO

775

776

777   HOMO

778

779

780

781   HOMO-1

782   VCTO1b   VCTO 2b   VCTO3b   VCTO4b

783

784

785

786

787   Figure 4

788

789

790

791

792

793

794

795

796

797
798
799
800
801
802
803
804
805
806
807
808
809
810
811
812
813
814
815
816
817
818
819
820
821
822
823
824
825
826
827
828
829
830

Band Gap = 12766.84-8553.99*β+1438.10*β²
(R²=0.9900)

Figure 5

831
832
833
834
835
836
837
838
839
840
841
842
843
844
845
846
847
848
849
850
851
852
853
854
855
856
857
858
859
860
861
862
863
864

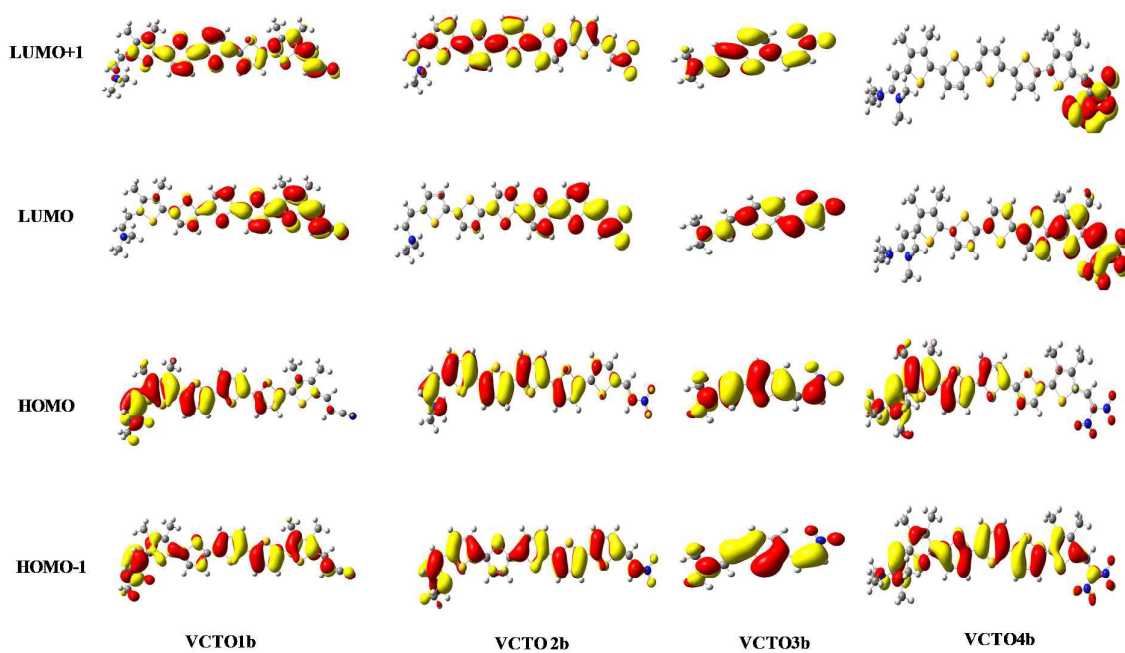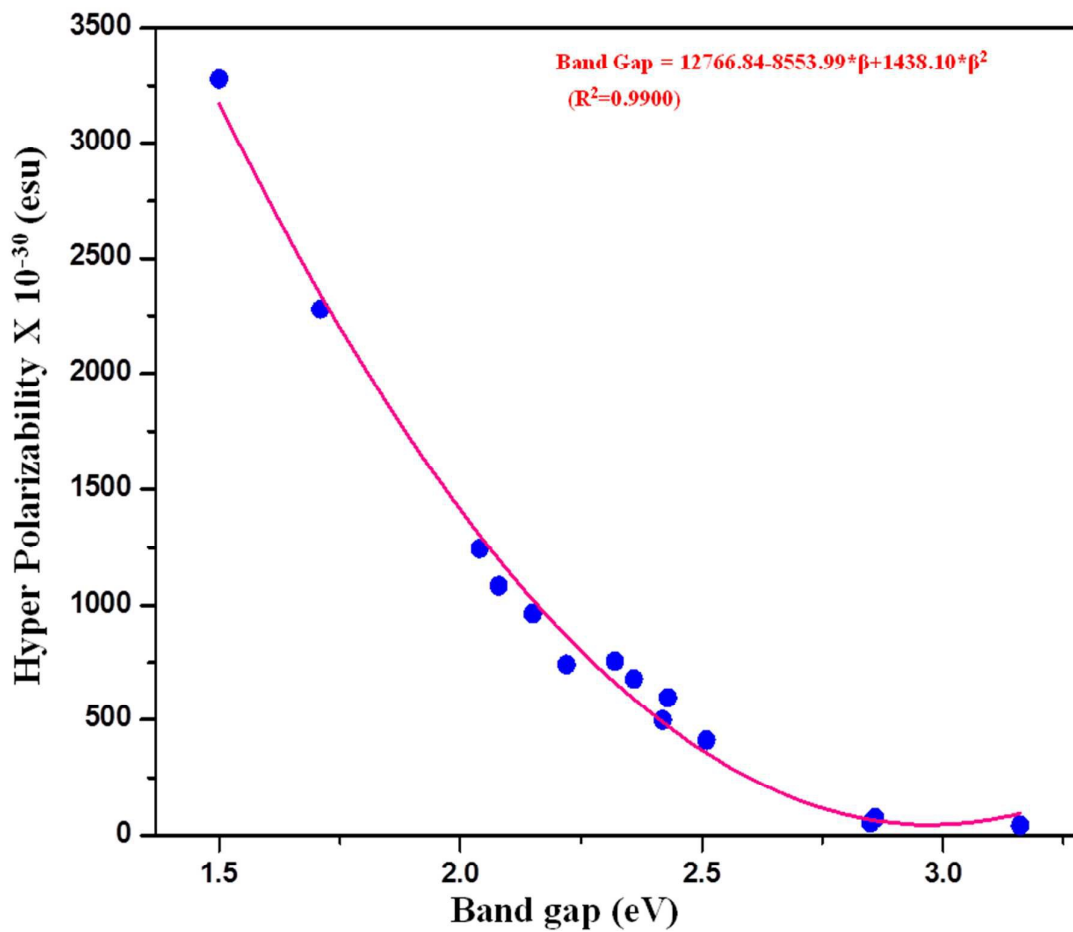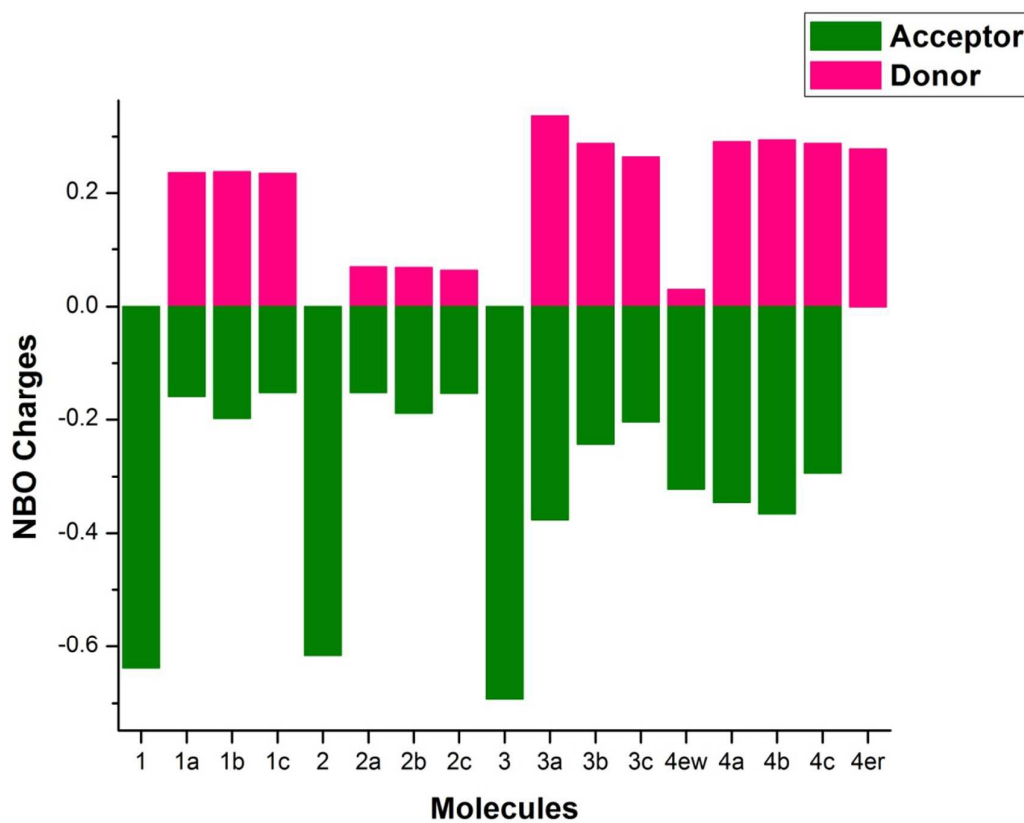**Figure 6**

865
866
867
868
869
870
871
872
873
874
875
876
877
878
879
880
881
882
883
884
885
886
887
888
889
890
891
892
893
894
895
896
897
898

	Donor	Acceptor	Donor-Acceptor interaction
VCTO1	π (C$_9$-C$_{36}$)	π*(C32-C39)	π (C$_9$-C$_{36}$) $\longrightarrow$ π*(C32-C39)
VCTO1a	LP(1) N$_{54}$	π * (C$_{11}$-C$_{18}$)	LP(1) N$_{54}$ $\longrightarrow$ π * (C$_{11}$-C$_{18}$)
VCTO1b	LP(3) O$_{64}$	π * (N$_{63}$-O$_{65}$)	LP(3) O$_{64}$ $\longrightarrow$ π * (N$_{63}$-O$_{65}$)
VCTO1c	LP(2) O$_{65}$	π * (C$_{63}$-O$_{64}$)	LP(2) O$_{65}$ $\longrightarrow$ π * (C$_{63}$-O$_{64}$)
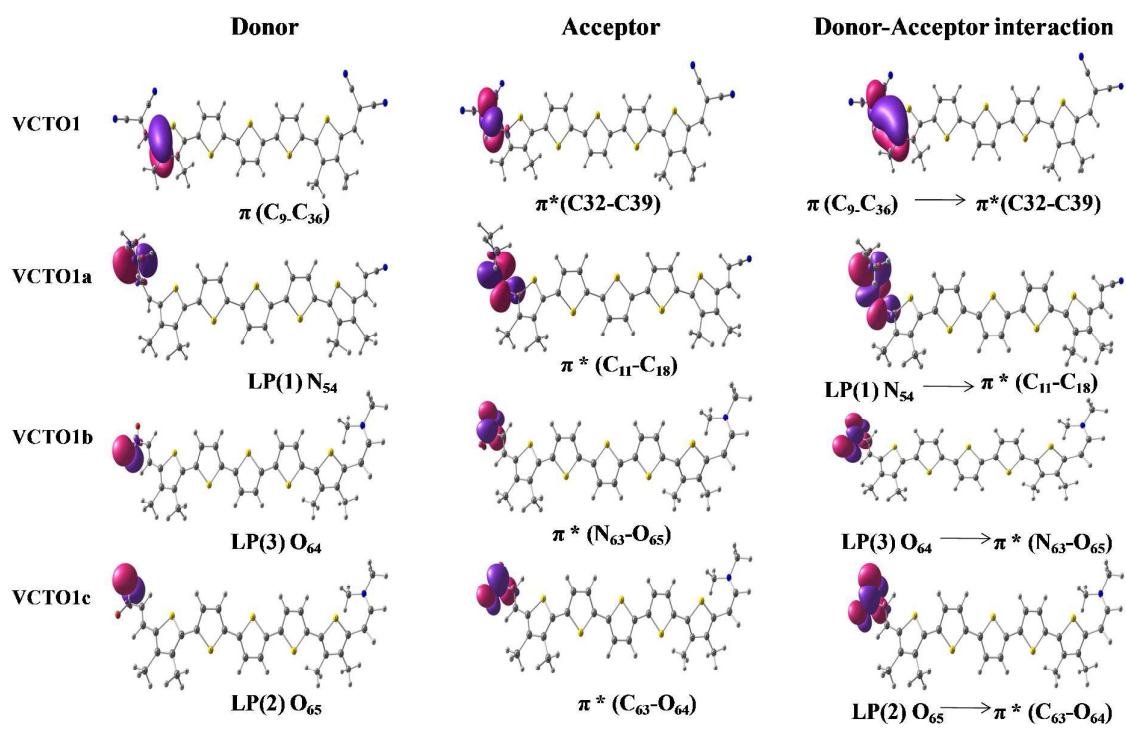
Figure 7

899

900

901

Molecules	Orbitals	π bridge	Donor	Acceptor	Methyl
	HOMO	86.94	0	11.51	1.55
VCTO1	LUMO	79.38	0	19.61	1.01
	HOMO	75.91	20.88	0.88	2.33
VCTO1a	LUMO	83.13	0.45	15.34	1.08
	HOMO	75.26	21.47	0.90	2.37
VCTO1b	LUMO	66.11	0.20	32.67	1.03
	HOMO	77.51	19.10	1.06	2.33
VCTO1c	LUMO	83.91	0.54	14.44	1.11
	HOMO	87.62	0	12.38	-
VCTO2	LUMO	80.94	0	19.06	-
	HOMO	86.54	11.18	2.28	-
VCTO2a	LUMO	85.44	1.11	13.45	-
	HOMO	84.88	13.12	1.99	-
VCTO2b	LUMO	70.85	0.46	28.67	-
	HOMO	86.66	10.96	2.36	-
VCTO2c	LUMO	85.38	1.26	13.28	-
	HOMO	43.16	0	56.84	-
VCTO3	LUMO	55.40	0	44.60	-
	HOMO	46.71	32.32	20.97	-
VCTO3a	LUMO	56.76	18.85	24.40	-
	HOMO	48.88	35.24	15.88	-
VCTO3b	LUMO	44.35	14.02	41.63	-
	HOMO	49.22	35.94	14.84	-
VCTO3c	LUMO	53.55	18.11	28.34	-
	HOMO	89.13	5.22	3.61	2.04
VCTO4ew	LUMO	77.63	0.21	21.00	1.16
	HOMO	70.35	26.38	0.79	2.48
VCTO4a	LUMO	77.05	0.39	21.37	1.19
	HOMO	69.49	27.17	0.85	2.49
VCTO4b	LUMO	64.96	0.29	33.65	1.09
	HOMO	71.69	25.12	0.67	2.52
VCTO4c	LUMO	77.14	0.42	21.12	1.32
	HOMO	73.22	23.74	0.53	2.52
VCTO4er	LUMO	93.40	1.98	3.68	0.94

902
903
904
905
906

Table 1: Frontier Molecular Orbital composition (%) by various fragments of the VCTOs optimized at B3LYP/6-31g(d) level.

907
908
909
910
911
912
913
914
915
916
917
918
919
920
921
922
923
924

925
926
927
928
929
930
931
932
933
934
935
936

937
938

Molecules	Dipole moment (Debye)		Hyperpolarizability (esu)
	Gas phase	CH$_2$Cl$_2$	
VCTO 1	12.16	16.13	50.93
VCTO1a	10.35	12.21	676.3
VCTO1b	11.47	13.73	1083
VCTO1c	6.61	7.59	595.05
VCTO2	9.37	13.23	44.8
VCTO2a	9.65	11.32	754.69
VCTO2b	11.19	13.42	963.55
VCTO2c	6.03	6.83	499.05
VCTO3	4.41	11.52	58.36
VCTO3a	12	15.95	55.5
VCTO3b	10.70	14.19	76.19
VCTO3c	4.41	5.39	43.69
VCTO4ew	11.44	14.38	740.90
VCTO4a	15.43	18.70	2280.90
VCTO4b	16.94	21.20	3278.83
VCTO4c	9.32	10.92	1242.28
VCTO4er	4.81	5.63	411.48

Table 2: Dipole moment in gas phase, DCM medium and calculated Hyperpolarizabilty values at B3LYP/6-31g(d) level.

949
950
951
952
953
954
955
956
957
958
959
960
961
962
963

36

Molecules	IP	EA	E_b
VCTO 1	5.51	3.19	-0.10
VCTO1a	4.67	2.31	-0.36
VCTO1b	4.72	2.64	-0.50
VCTO1c	4.63	2.20	-0.29
VCTO2	5.64	3.40	-0.10
VCTO2a	4.90	2.58	-0.25
VCTO2b	4.98	2.83	-0.35
VCTO2c	4.86	2.43	-0.22
VCTO3	7.11	4.08	-0.11
VCTO3a	5.31	2.45	0.13
VCTO3b	5.14	2.27	0.10
VCTO3c	4.73	1.5	0.08
VCTO4ew	5.13	2.91	-0.45
VCTO4a	4.49	2.78	-0.67
VCTO4b	4.53	3.02	-0.78
VCTO4c	4.41	2.36	-0.55
VCTO4er	4.31	1.80	-0.29

Table 3: Calculated ionization potential (IP), electron affinity (EA) and exciton binding energy (E_b) at B3LYP/6-31g(d) level for VCTOs in eV.

1007

1008

1009

1010

1011

| Molecules | λ_{max} (gas phase) | | f | Transition assignments |
	nm	eV		
VCTO 1	404	3.07	2.74	H → L (85%)
VCTO1a	361	3.44	2.39	H → L (62%)
VCTO1b	462	2.69	2.04	H → L (55%) H-1→ L (20%) H→ L+1(18%)
VCTO1c	442	2.81	2.14	H→ L (66%)
VCTO2	415	2.99	2.96	H→L (87%)
VCTO2a	468	2.65	2.29	H→ L (76%)
VCTO2b	475	2.61	2.20	H→ L (68%)
VCTO2c	455	2.73	2.30	H→ L (77%)
VCTO3	371	3.35	1.13	H→ L (99%)
VCTO3a	412	3.01	0.89	H→L (99%)
VCTO3b	399	3.11	0.94	H→L (97%)
VCTO3c	373	3.32	0.72	H→L (98%)
VCTO4ew	476	2.60	1.98	H→ L (74)
VCTO4a	522	2.38	1.89	H→L (60%) H-1→ L (21%)
VCTO4b	545	2.28	1.68	H→L (64%) H-1→L (19%)
VCTO4c	476	2.6	2.14	H→L (53%) H-1→L (21%) H→L+1(20%)
VCTO4er	444	2.80	2.00	H→ L (74%)

1012

1013 **Table 4:** Absorption maxima (λ_{max}), electronic transition energies (ΔE), oscillator strength (f), light harvesting efficiency (LHE) and
1014 transition assignments of VCTOs in gas phase from TDDFT calculations at MO62X/6-31g(d) level.

1015

1016

1017

1018

1019

1020

1021

1022

1023

1024

1025

1026

1027

1028

1029

1030

1031

1032

1033

1034

1035

1036

1037

1038

1039

1040

1041

1042

1043

1044

1045

1046

1047

1048

1049

Molecules	λ_{max} (DCM)		f	LHE	Transition assignments
	nm	eV			
VCTO 1	513(527)	2.42	2.64	0.997	H→L (83%) H-1→ L+1(11%)
VCTO1a	455	2.72	2.31	0.995	H→L (58%) H-1→L (20%) H→L+1(15%)
VCTO1b	481	2.58	2.22	0.994	H→L (48%) H-1→L (24%) H→L+1(19%)
VCTO1c	456	2.72	2.30	0.995	H→L (61%) H-1→L (19%) H→L+1(14%)
VCTO2	532 (530)	2.33	2.81	0.998	H→L (85%) H-1→L+1(10%)
VCTO2a	483	2.57	2.48	0.996	H→L (76%) H→L+1(9%) H-1→L(8%)
VCTO2b	495	2.5	2.40	0.996	H→L (65%) H→L+1(15%) H-→L(15%)
VCTO2c	470	2.64	2.47	0.996	H→L (76%) H→L+1(9%) H-1→L (8%)
VCTO3	394(406)	3.14	0.91	0.878	H→L (99%)
VCTO3a	456	2.72	1.03	0.907	H→L (98%)
VCTO3b	449	2.76	1.07	0.916	H→L (96%)
VCTO3c	402	3.08	0.83	0.852	H→L (97%)
VCTO4ew	499	2.49	2.11	0.992	H→L(73%) H-1→ L (15%) H→L+1(8%)
VCTO4a	544	2.28	2.10	0.992	H→L(55%) H-1→L(25%) H→L+1(14%)
VCTO4b	576	2.15	1.84	0.985	H→L(59%) H-1→ L (24%) H→L+1(8%)
VCTO4c	496	2.50	2.29	0.994	H→L(48%) H-1→L(23%) H→L+1(21%)
VCTO4 er	461	2.69	2.09	0.991	H→L(72%) H-1→L(11%) H→ L+1(9%)

1050

1051

1052

1053

1054

1055

1056 **Table 5:** Absorption maxima (λ_{max}), electronic transition energies (ΔE), oscillator strength (f) and transition assignments of VCTOs in DCM
1057 medium from TDDFT calculations at MO62X/6-31g(d) level.

1058

1059

1060

1061

1062

1063

1064

1065

Molecules	Donor (i)	ED(i) (e)	% ED Polarization	Orbital Energy(au)	Acceptor(j)	ED(j) (e)	%ED Polarization	Orbital Energy(au)	E(2) kcal/mol	Ej-Ei
VCTO1	π (C_9-C_{36})	1.7076	57.10 C_9-42.90 C_{36}	-0.2516	π*(C32-C39)	0.2833	59.07C_{32}-40.93 C_{39}	0.0462	26.50	0.28
VCTO1a	LP(1) N_{54}	1.7016	-	-0.2408	π * (C_{11}-C_{18})	0.2437	44 C_{11}-56 C_{18}	0.0544	39.86	0.30
VCTI1b	LP(3) O_{64}	1.4822	-	-0.2549	π * (N_{63}-O_{65})	0.6520	59.96N_{63}-40.04 O_{65}	-0.1153	154.88	0.14
VCTO1c	LP(2) O_{65}	1.8240	-	-0.3181	π * (C_{63}-C_{64})	0.2910	70.35 C_{63}-29.65 O_{64}	0.0188	44.79	0.34
VCTO2	π($C_{31}$$C_{39}$)	1.7173	56.38C_{31}-43.62 C_{39}	-0.2971	π * (C_{34}-O_{13})	0.2787	58.85 C_{34}-41.15 O_{13}	-0.0079	26.10	0.29
VCTO2a	LP(2) S_2	1.6710	-	-0.2607	π * (C_{13}-C_{14})	0.3685	48.44 C_{13}-51.56 C_{14}	0.0049	21.31	0.27
VCTO2b	LP(3) O_{53}	1.4781	-	-0.2578	π * (N_{51}-O_{52})	0.6508	59.88N_{51}-40.12 O_{52}	-0.1185	156.27	0.14
VCTO2c	LP (2)O_{52}	1.8232	-	-0.3210	π * (C_{51}-O_{53})	0.2880	70.21 C_{51}-29.79 O_{53}	0.0161	44.92	0.34
VCTO3	LP(2) S_1	1.6041	-	-0.2911	π * (C_6-C_7)	0.3856	45.65 C_6-54.35 C_7	-0.0385	23.07	0.25
VCTO3a	LP(1) O_{24}	1.6634	-	-0.2718	π * (C_2-C_{11})	0.2844	42.66 C_2-57.34 C_{11}	0.0151	49.71	0.29
VCTO3b	LP(3)O_{24}	1.4942	-	-0.2491	π * (N_{23}-O_{25})	0.6712	60.42N_{23}-39.58 O_{25}	-0.1076	146.51	0.14
VCTO3c	LP(2) O_{25}	1.8289	-	-0.3103	π * (C_{23}-O_{24})	0.3090	70.96 C_{23}-29.04 O_{24}	0.0237	43.86	0.33
VCTO4ew	π (C_8-C_{15})	1.7050	57.23C_8-42.77 C_{15}	-0.2819	π * (C_{11}-C_{18})	0.2914	59.26 C_{11}-40.74 C_{18}	0.0014	27.02	0.28
VCTO4a	LP(1) N_{59}	1.7564	-	-0.2575	π * (C_{32}-C_{39})	0.3297	43.13 C_{32}-56.87 C_{39}	0.0387	27.94	0.30
VCTO4b	LP(3) O_{77}	1.4807	-	-0.2701	π * (N_{75}-O_{76})	0.6335	59.01N_{75}-40.99 O_{76}	-0.1232	148.24	0.15
VCTO4c	LP(2) O_{74}	1.8092	-	-0.317	π * (C_{72}-O_{73})	0.2862	70.85 C_{72}-29.15 O_{73}	0.0133	48.59	0.33
VCTO4er	LP(1) N_{55}	1.7606	-	-0.2516	π * (C_{28}-C_{35})	0.3255	43.23 C_{28}-56.77 C_{35}	0.0462	27.62	0.30

1066

1067 **Table 6:** Stable NBO donor-acceptor interactions of VCTOs with its occupancy, %ED, and O.E obtained from B3LYP/6-31g(d)
1068 calculations. E (2) is the energy of hyper conjugative interaction. ED is the electron density; Ej-Ei is the energy difference between donor (i)
1069 and acceptor (j) NBO orbitals.

1070

1071

1072

1073

1074

1075

1076

1077

1078

1079